### ORIGINAL RESEARCH



# Waterborne functionalization of cellulose nanofibrils with norbornenes and subsequent thiol-norbornene gelation to create robust hydrogels

Nayereh Dadoo · Sarah Zeitler · Ashlee D. McGovern · William M. Gramlich

Received: 21 July 2020/Accepted: 11 November 2020

© Springer Nature B.V. 2021

Abstract Cellulose nanofibrils (CNFs) produced through processes involving oxidation (e.g. TEMPO oxidation) present reactive groups that allow for straightforward modification in aqueous suspension. CNFs fabricated through mechanical refinement alone can be challenging to modify for subsequent reactions due to only having hydroxyl groups present on the surface. To address these issues, CNFs with only hydroxyl groups present were functionalized with norbornene groups in their native aqueous suspension to achieve up to 10% functionalization per anhydroglucose unit. Since quantification of surface functionalization of CNFs is challenging through most

**Electronic supplementary material** The online version of this article (https://doi.org/10.1007/s10570-020-03582-z) contains supplementary material, which is available to authorized users.

N. Dadoo · S. Zeitler · A. D. McGovern ·

W. M. Gramlich (⊠)

Department of Chemistry, University of Maine, Orono, ME 04469, USA

e-mail: william.gramlich@maine.edu

Present Address:

S. Zeitler

Department of Chemistry, University of Washington, Seattle, WA, USA

Present Address:

A. D. McGovern
Department of Chemistry, Penn State University,

State College, PA, USA

Published online: 03 January 2021

methods, a degradation and subsequent nuclear magnetic resonance analysis method was developed to quantify norbornene functionalization. The norbornene functionalized CNFs (nCNFs) were crosslinked through UV and thermally initiated thiol-ene click reactions to create robust CNF hydrogels. By varying the reaction conditions, hydrogels made from nCNFs and a dithiol cross-linker could achieve compression modulus values up to 25 kPa. The materials were stable in aqueous suspensions and the cross-linked hydrogels still exhibited shear thinning behavior with high recovery, which demonstrated that even though effective cross-links were formed, a complete network was not. Through this study, thiolnorbornene crosslinking of CNFs could create robust hydrogels and improve aqueous stability that could have applications in sustainable materials and biomaterials.

**Keywords** Cellulose nanofibrils · Colloidal hydrogels · Thiol-ene reaction · Shear thinning hydrogels · Mechanically refined cellulose nanofibrils

#### Introduction

Cellulose nanofibrils (CNFs) are interesting renewably sourced nanomaterials due to their nanometer scale widths and high aspect ratio (Oksman et al.



2009). Significant differences do exist between the mechanically ground CNFs without oxidative pretreatment as compared to carboxylic acid functionalized (TEMPO oxidized or carboxymethylated) CNFs (Spence et al. 2011). Mechanically ground CNFs without oxidative pretreatment (OH-CNFs) tend to have more hierarchical structures (Berto and Arantes 2019; Espinosa et al. 2019), larger diameters (Nechyporchuk et al. 2015), and only have hydroxyl groups on the fibril surface (Otoni et al. 2018). OH-CNFs have been used as mechanical reinforcements in nanocomposites (Deng et al. 2016; Kargarzadeh et al. 2018), as the main component of porous materials (Gordeyeva et al. 2016; Mariano et al. 2018; Zhang et al. 2019), as thin films (Sharma et al. 2018; Hoeng et al. 2016; Deng et al. 2017), and in numerous other applications (Moon et al. 2011, 2016). However, CNFs have high water content (> 90%) and are difficult to dewater, which can make implementing them in dry applications difficult.

CNF dispersions exhibit shear thinning, gel-like character in aqueous media even at concentrations as low as 0.1 wt% due to hydrogen bonding (De France et al. 2017) and have been utilized as scaffolds for tissue engineering because their fibril structure mimics the hierarchical, fibrous components of the extracellular matrix (ECM) (Martin-Martinez et al. 2018; Curvello et al. 2019). Physical CNF hydrogels have been created from carboxylic acid functionalized CNFs (Fu et al. 2019; Dong et al. 2013; Basu et al. 2018; Liu et al. 2016; Zander et al. 2014) and these oxidized CNFs have been chemically crosslinked as well (Syverud et al.2011, 2015; Nishiguchi and Taguchi 2019; Erlandsson et al. 2018). However, OH-CNFs yield physical hydrogels and have been incorporated into other polymer networks (De France et al. 2017; Kong et al. 2018; Doench et al. 2018; Yang et al. 2018; Yang and Xu 2017; Heggset et al. 2019; Campodoni et al. 2019; Xu et al. 2019a, b; Niu et al. 2018), but OH-CNFs, to the authors' knowledge, have not been directly chemically crosslinked to each other to create robust hydrogels. Nevertheless, hydrogels and suspensions made from OH-CNFs have been used to culture mammalian cells (Lou et al. 2014; Bhattacharya et al. 2012; Azoidis et al. 2017; Mathew et al. 2012; Tomic et al. 2016) with low cytotoxicity, which demonstrate their potential biomedical application as a shear thinning suspension. Chemical stabilization of OH-CNF hydrogels could lead to new applications as self-standing, only OH-CNF cell scaffolds.

To improve the stability and mechanical properties with chemical cross-linking, suitable functional groups are necessary (Rol et al. 2019). Surface modifications to carboxylic acid functionalized CNFs have been done in their native aqueous suspension through activating the carboxylic acid towards acyl substitution reactions (Chin et al. 2018). Such surface modifications can change the cytotoxicity of CNFs, but in general modified CNFs remain cytocompatible (Rashad et al. 2017). In contrast, most of the modifications to OH-CNFs are done in organic solvents due to the low relative reactivity of the surface hydroxyl groups as compared to the surrounding water (Navarro and Edlund 2017). The transfer between aqueous and organic conditions is possible through solvent exchanges, but these can lead to CNFs aggregation and the need for thorough purification prior to biological studies (Vuoti et al. 2013). Straightforward methods are needed to place reactive groups on the surface hydroxyl functionalized CNFs in water. Some examples of these types of modifications exist to CNFs (Saini et al. 2016; Satyamurthy et al. 2016; Wang et al. 2016; Khalil et al. 2014) and water-soluble polysaccharides that can serve as starting points for new chemistry to enable covalent cross-linking of CNFs (McOscar and Gramlich 2018). Our laboratory recently demonstrated that we could functionalize CNFs with norbornenes in water for subsequent surface modifications (Fein et al. 2020).

Highly controlled cross-linking chemistries can enable new applications of CNF hydrogels through tuning of mechanical, stability, and degradation properties. So called 'click' and light initiated reactions have been used with polysaccharides to yield spatiotemporal control over physical properties and chemical presentation that can be beneficial for biomedical applications (McOscar and Gramlich 2018; Dadoo et al. 2017). Though the azide-alkyne click reaction has been used to cross-link carboxylic acid functionalized cellulose nanocrystals (CNCs) (Filpponen and Argyropoulos 2010), this and other click reactions such as thiol-ene have yet to be used extensively to form robust CNF hydrogels. Thiol-ene reactions are radical catalyzed, which enable spatiotemporal control of properties in hydrogels when a light sensitive initiator is used (Brown and Anseth 2017). Moreover, since the thiol-ene reactions create a



one-to-one linkage between species, specific enzymatic activity can be programmed into the cross-linker and thiol-functionalized molecules to control cell fate (Ooi et al. 2017). Thiol-ene and more specifically thiol-norbornene cross-linked hydrogels have been implemented in many water-soluble polysaccharide hydrogels (Lin et al. 2015; McCall and Anseth 2012; Jivan et al. 2016; dadoo et al. 2017; Gramlich et al. 2013; Caliari et al. 2016), suggesting that if such chemistry could be developed with CNFs, new biomaterials could be realized.

In this work, we build upon our previous work (Fein et al. 2020) to functionalize OH-CNFs with norbornene groups in a straightforward aqueous reaction by demonstrating control over the degree of functionalization. To accurately quantify the degree of norbornene functionalization, a method was developed and optimized to perform <sup>1</sup>H-NMR spectroscopy on the CNFs after enzymatic hydrolysis. Norbornene functionalized CNFs (nCNFs) were cross-linked by thiol-norbornene chemistry using different dithiol cross-linkers and initiator systems, which demonstrated control over the compression and storage modulus of the hydrogels to give a visible increase in stability of the constructs in aqueous media. Though cross-linked to some extent, some hydrogels retained their shear thinning nature. By demonstrating and characterizing several methods to crosslink these hydrogels, we lay the foundation for future work implementing these materials in biomaterial and sustainable material applications.

## Materials and methods

#### Materials

Cellulose nanofibrils (CNFs) were produced at the University of Maine Process Development Center through mechanical refining of softwood bleached kraft pulp to give an aqueous dispersion with 3 wt% solid content at 90% fines. To determine the average diameter of cellulose fibers, diluted CNFs (0.04 wt% in deionized water) were dropped on a copper TEM grid, evaporated, and stained with uranyl acetate as a negative dye. Images on the sample grid sample were collected using transmission electron microscopy (TEM) (CM10, Philips) and the Gatan microscopy software (v2.31). ImageJ software was used to

measure the diameter of fibrils that intersected with a 10X10 grid. The average diameter was found to be  $120 \pm 20$  nm, which is consistent with previous results using these materials that also indicate fibril lengths on the micrometer scale (Salari et al. 2019). The reagent 5-norbornene-2,3-dicarboxylic anhydride (NB) was purchased from TCI America. Other reagents and polymers such as 2-hydroxy-4'-(2-hydroxyethoxy)-2-methylpropiophenone (I2959), 2,2'-(ethylenedioxy) diethanethiol (DTDEG), poly(ethylene glycol)dithiol with an M<sub>n</sub> of 1500 g/mol (DTPEG 1.5 k), poly(ethylene glycol)dithiol with an M<sub>n</sub> of 3400 g/mol (DTPEG 3 k), and N,N,N',N'-tetramethylethylenediamine (TEMED) were purchased from Sigma-Aldrich. Ammonium persulfate (APS) was purchased from Acros Organic. Cellulase (recombinant hydrolase enzymes) from Tricoderma Reesei was purchased from Sigma-Aldrich. All reagents were used without purification unless otherwise noted.

Synthesis of norbornene functionalized CNF (nCNF)

In a representative synthesis, 33 g of 3 wt% solids CNFs (6 mmol of anhydroglucose repeat units) were dispersed in 67 mL of deionized water to obtain 1 wt% CNF dispersion. To this dispersion, 19.73 g of 5-norbornene-2,3-dicarboxylic anhydride (120 mmol, 20 molar excess to repeat units) was added, which caused the pH to drop to 4. Sodium hydroxide (NaOH) 10 M solution was added dropwise to bring up and keep the pH between 9.5-10.5 throughout the reaction. The pH decrease slowed down as the reaction completed and stopped changing after 2.5 h. The product was washed with DI water five times via centrifugation at 7000 rpm for 15 min using a SORVALL RC-6 PLUS centrifuge (Thermo Electron Corporation) and SLA-1500 rotor. The final product, norbornene functionalized CNFs (nCNFs), was at 2.7 wt% solids after the fifth wash. This synthesis was repeated varying the concentration of 5-norbornene-2,3-dicarboxylic anhydride (0.13, 0.3, 0.6, and 1.2 M) to obtain nCNFs with different degrees of functionalization.

Analysis of nCNF functionalization by IR spectroscopy

Attenuated total reflectance-Fourier transform infrared (ATR-FTIR) spectroscopy was used to probe the



presence of norbornene (NB) functional groups on nCNFs and obtain a relative ratio of absorption bands corresponding to different functional groups. The nCNF dispersion was lyophilized prior to ATR-FTIR spectroscopy (PerkinElmer UATR Two, diamond crystal). Spectra were collected from 450 to 4000 cm<sup>-1</sup> at 1 cm<sup>-1</sup> resolution and spectra were taken in triplicate. A peak area ratio between the C–O band of cellulose (1212–915 cm<sup>-1</sup>) and new bands corresponding to the functional groups associated with the norbornene (1765–1495 cm<sup>-1</sup>) was calculated by integrating under the curves in the absorbance spectra. See Fig. S1 for a schematic of the integration of the ATR-FTIR spectra of nCNFs.

Analysis of nCNF functionalization by <sup>1</sup>H-NMR spectroscopy

To quantify the degree of norbornene functionalization on nCNFs by proton nuclear magnetic resonance (<sup>1</sup>H-NMR) spectroscopy, the samples were enzymatically degraded to enable analysis. The enzymatic degradation process was optimized to achieve a high percent of degradation into glucose monomers. Table S1 gives details of parameters explored and the resulting degradation of CNFs into glucose. For each analysis, an initial CNF or nCNF dispersion was diluted using sodium acetate/acetic acid buffered solution (pH 5) to prepare 1 mL of 1 wt% dispersion. In a representative and optimized measurement, 0.27 g of 3.7 wt% CNF was redispersed in 730 µL buffer. To this dispersion, 10 µL of cellulase enzyme was added and incubated at 50 °C after vortex mixing for few seconds. After 18 h, a second dose of enzyme was added and incubated for 2 h. The degraded sample was freeze-dried and redispersed in 0.65 mL of D<sub>2</sub>O for <sup>1</sup>H-NMR spectroscopy. To degrade nCNF hydrogels, the procedure was slightly modified so that 1 mL of sodium acetate buffer was added to a 50 µL hydrogel initially with the rest of the procedure continuing as above. All <sup>1</sup>H-NMR spectra were obtained on a Varian Inova 400 MHz spectrometer. <sup>1</sup>H-NMR spectroscopy of degraded CNFs (D<sub>2</sub>O, 400 MHz) δ: 1.88 ppm (acetate -CH<sub>3</sub>, singlet, 3H), 3-4 ppm (glucose and various polysaccharides, broad multiple peaks), 4.61 ppm (β-anomeric proton, doublet, 1H), and 5.20 ppm (α-anomeric proton, doublet, 1H). <sup>1</sup>H-NMR spectroscopy of nCNF (D<sub>2</sub>O, 400 MHz) δ: 1.35 ppm (norbornene bridge -CH<sub>2</sub>, multiplet, 2H) 1.88 ppm (acetate -CH<sub>3</sub>, singlet, 3H), 3.12 ppm (norbornene bridge head -CH, singlet, 2H), 3–4 ppm (glucose and various polysaccharides, broad multiple peaks), 4.61 ppm ( $\beta$ -anomeric proton, doublet, 1H), 5.20 ppm ( $\alpha$ -anomeric proton, doublet, 1H), and 6.20 ppm (norbornene vinyl protons, singlet, 2H).

To calculate the degree of norbornene functionalization using <sup>1</sup>H-NMR spectroscopy, the acetate peak at 1.88 ppm (from the known quantity of buffer) was used as internal standard. The acetate peak integration was compared to the overall integration of the anomeric proton peaks at 4.61 and 5.20 ppm to give the percent degradation into glucose. Under optimized conditions, CNFs and nCNFs degraded to 85% glucose and this was used to correct the calculated degree of functionalization. With this information, the overall integrations of the anomeric hydrogen peaks and the integration of norbornene double bond peak at 6.20 ppm were used to calculate the degree of norbornene functionalization on an anhydroglucose repeat unit basis. See Supporting Information for equations and more detailed explanation.

## Cross-linking nCNFs

To cross-link nCNFs, the original 2.7 wt% solids nCNFs was centrifuged to remove water until a 4 wt% nCNF suspension was obtained. Hydrogels were formed at various molar ratios of thiol to norbornene (T/NB), cross-linker molecules, and radical generation systems. To prepare the pre-hydrogel dispersion, 4 wt% nCNFs and cross-linker were vortex mixed for 20 min followed by mechanical stirring. For UV-light initiated gelation, the radical initiator 2-hydroxy-4'-(2-hydroxyethoxy)-2-methylpropiophenone (I2959) (0.05 wt% in pre-hydrogel dispersion) was added and mechanically mixed into the dispersion. Portions of solution (50 µL) were transferred by a spatula to 1 mL syringes with the top cut off. The solution was covered with coverslip (0.22 mm thickness) and irradiated with 365 nm light (Omnicure S1000 UV lamp filtered for 320–390 nm) at 10 mW/cm<sup>2</sup> power for 20 min. For thermal gelation, to the 4 wt% nCNFs/ cross-linker dispersion, APS and TEMED stock solutions were added so that their final concentrations were 10 mM in the dispersion. After vortex mixing and mechanical mixing, 50 µL portions of the dispersion were transferred to 1 mL syringes with the top cut off, sealed with glass coverslips, and



incubated at 37  $^{\circ}$ C for 3 h. All hydrogels were stored in 1 mL PBS for 24 h at 4  $^{\circ}$ C prior to subsequent testing.

# Measuring compression modulus

A dynamic mechanical analyzer (DMA) (Q8000 Thermal Analysis) with a compression fixture was used to measure the compression moduli of the hydrogels. After incubating at 37 °C for 24 h in PBS, the 50  $\mu$ L hydrogels (n  $\geq$  4) were subjected to a constant compression strain rate experiment at 10% strain/min up to 30% total strain. Compression modulus was defined as the slope of strain–stress curve in the limit of 10 to 20% compressive strain. The degree of swelling was estimated by measuring the change in diameter (assuming isotropic swelling) after incubating at 37 °C for 24 h as compared to the diameter of the mold and dividing by the diameter of the mold.

## Rheology measurements

The storage modulus of some formulations were obtained from rheological experiments using a TA Discovery HR-2 rheometer with a 40 mm aluminum cone-plate geometry with a 2° angle and a 60 µm gap. CNF and nCNF dispersions with total volume of 620 µL were transferred to an aluminum Pelletier plate at 37 °C. To perform rheological measurements on nCNF-DTDEG hydrogels, 620 µL nCNF-DTDEG (3 and 4 wt%) dispersion with 10 mM of APS and TEMED (for thermal radical generation) and T/NB equal to one, was transferred to the Peltier plate, enclosed from the sides with a rubber mold, and covered with the rheometer geometry. Samples were incubated for 3 h at 37 °C prior to testing. For all rheology measurements, water droplets were placed around the geometry and the system was covered with a solvent trap to keep the surrounding humid to assure that hydrogels did not dry out during the run.

Time sweep measurements were run in the linear response regime at 37 °C, 1 Hz oscillatory frequency, and 1% oscillatory strain for one hour. Oscillatory strain sweeps (0.05–250%) were conducted at 37 °C and 1 Hz oscillatory frequency. Modulus recovery after shear-thinning was done at 37 °C and a constant oscillatory frequency (10 Hz) with alternating amplitude of oscillatory strain between 0.5 and 250% strain.

A higher frequency was selected to demonstrate more significant changes between solid and liquid like behavior (Rodell et al. 2013). An initial time sweep at 0.5% strain was run for 5 min on each dispersion to equilibrate the sample. After the initial low strain run, high strain (250% strain) was applied for 2 min immediately followed by a low strain (0.5% strain) run for 2 min. This alternating high/low strain was repeated two additional cycles.

#### Results and discussion

## Functionalization of CNF

The norbornene functional group was successfully added to mechanically produced CNFs through an esterification reaction between the available hydroxyl groups on the surface of CNFs and the anhydride of 5-norbornene-2,3-dicarboxylic anhydride in aqueous dispersion (Fig. 1a). These hydroxyl groups could be from both cellulose and adsorbed hemicelluloses that remain after kraft pulping. Once added to the dispersion, the anhydride readily reacted with free hydroxyl groups on CNFs to form the ester linkage and also a free carboxylic acid. Additionally, an unwanted side reaction occurs where the anhydride hydrolyzes to form the norbornene-2,3-dicarboxylic acid small molecule. Both this hydrolysis and coupling contribute to a dramatic pH drop, which required titration with NaOH throughout the reaction to keep the pH between 9.5 and 10.5. This range was selected as previous work in our group with this anhydride and carboxymethyl cellulose (CMC) yielded the highest functionality (McOscar and Gramlich 2018). A NaOH concentration of 10 M was used so that base addition would not change the reaction volume appreciably. The reaction was somewhat pH sensitive where a pH below 7 led to no reaction and if the pH was 13 or more, all the anhydrides hydrolyzed, which led to no CNF functionalization. After 2 h, the reaction slowed considerably as demonstrated by the slow rate of base addition and was considered complete when the pH was stable for 30 min. Since the nCNF product was not soluble in water and the only impurity was water soluble norbornene-2,3-dicarboxylic acid, purification was accomplished by five washes with deionized water using centrifugation. This straightforward reaction and purification processes are expected to be possible at higher volumes (Fein et al. 2020).



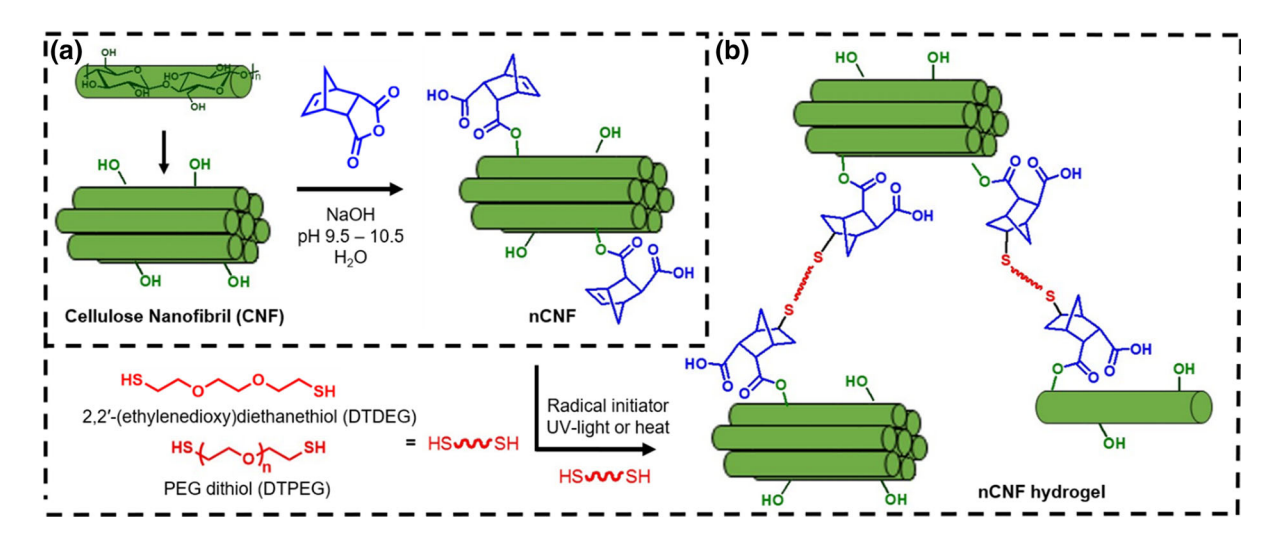


**Fig. 1** a Schematic of the surface functionalization of cellulose nanofibrils (CNFs) with 5-norbornene-2,3-dicarboxylic anhydride in aqueous media and at controlled pH. **b** Schematic of

chemical cross-linking between fibrils of nCNFs via radical initiated thiol-norbornene reaction to fabricate nCNF hydrogels

The covalent attachment of the norbornene group to CNFs to create nCNFs was confirmed through ATR-FTIR spectroscopy of freeze dried samples. As shown in Fig. 2a, the spectrum of freeze-dried nCNFs had three new bands appear at 1560, 1630, and 1720 cm<sup>-1</sup> that belonged to carboxylate, norbornene double bond, and ester groups, respectively. The band at 1630 cm<sup>-1</sup> could be observed sometimes in the original CNF spectra after freeze-drying, which has been reported

due to adsorbed water and suggests that some of the signal at this wavenumber could be coming from this as well in the nCNFs (Lojewska et al. 2005; Yuan et al. 2017). Both a band from the ester and a carboxylate were expected with covalent bonding of the norbornene group due to the ring opening of the anhydride to produce the ester linkage (Fig. 1). Large carboxylate bands relative to the ester bands indicated free dicarboxylic acid as opposed to the bound functional

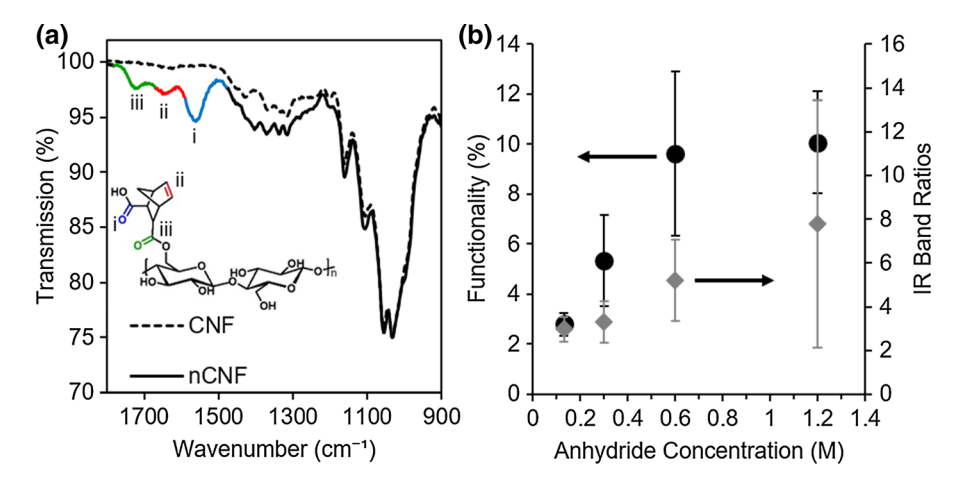


**Fig. 2 a** ATR-FTIR spectra of CNFs before (dash) and after (solid) functionalization with norbornene groups to produce nCNFs. Bands are color coded to the assigned functional groups in the inset structure to indicate (i) ester, (ii) alkene, and (iii) carboxylate functional groups. **b** The relation between anhydride concentration and norbornene functionalization on nCNFs measured from <sup>1</sup>H-NMR spectroscopy using enzymatic

degradation of nCNFs (left axis, black circles) to give percent anhydroglucose repeat unit functionality and ATR-FTIR spectroscopy to give band ratios (right axis, grey diamonds) based of the C–O peak area (1212–915 cm<sup>-1</sup>) divided by peak area of bands corresponding to the functional groups associated with the norbornene (1765–1495 cm<sup>-1</sup>). Error bars represent the standard deviation of three samples



group as was used to assess whether washing steps were effective. Under the centrifugation processes used, five washes were enough to remove the unbound molecules as indicated by its unchanging height relative to the ester band. This purification strategy is advantageous because water is the only solvent used and it yields the purified product in an aqueous dispersion, which prevents irreversible hydrogen bonding (i.e. hornification) that occurs during drying processes such as freeze drying that prevent efficient re-dispersion (Diniz and Castro 2004; Kato et al. 1999).

### Quantification of norbornene functionalization

The degree of norbornene functionality on nCNFs was controlled by varying the molarity of added anhydride (Fig. 2b) as inferred by ATR-FTIR spectroscopy on dried samples. The band area ratio of the backbone band to the functional group band increased from 3 to 8 as anhydride concentration increased from 0.13 to 1.2 M, demonstrating that the relative concentration of norbornene functional groups on nCNFs could be increased with anhydride concentration. However, the samples made with 1.2 M of anhydride were highly variable, suggesting that using 0.6 or 1.2 M anhydride concentration did not significantly affect the degree of functionalization because of error bars overlapping with the averages. The additional signal from the adsorbed water or perhaps remaining impurities from hydrolyzed anhydride may have led to the larger variability seen at the higher functionalization as measured by ATR-FTIR. If concentrations above 0.6 M could not change CNF functionalization, the CNF surfaces may have been completely saturated with norbornenes at this concentration.

Since the degree of functionalization information obtained using infrared spectroscopy is relative and not absolute, a method was desired to quantify the concentration of norbornene groups in the nCNF suspension. Quantification of the degree of functionalization of CNFs in previous work has been challenging since CNFs are not soluble in common NMR solvents and solid state <sup>13</sup>C-NMR spectroscopy of CNFs often gives qualitative information (Courtenay et al. 2018); though, it can be quantitative under the correct conditions (Bozic et al. 2015). Ideally, techniques such as <sup>1</sup>H-NMR spectroscopy could be used to more clearly and straightforwardly quantify the degree

of functionalization, but the modified CNF needs to be soluble for solution state NMR spectroscopy. Thus, using the method from our previous work (Fein et al. 2020), we degraded CNFs and their derivatives into water soluble sugar units using a mixture of enzymes (cellulase) that hydrolyze glycoside bonds.

Our previous work did not optimize the degradation and analysis process so we further validated and optimized the method to track how anhydride concentration affected CNF functionalization. CNF was degraded to water soluble segments with enzymatic treatments with recombinant hydrolase enzymes (cellulase) from Tricoderma reesei, which are mixture of enzymes with different target sites (Vinzant et al. 2001). Enzymatic treatment should yield glucose, cellobiose, and glucose oligomers according to the manufacturer and is most effective at pH 5 and a temperature range of 40-60 °C so that enzymes that degrade crystalline regions are effective (Shinner and Mersi 1990; Balasubramanian and Nelson 2014; Wang et al. 2017). However, long term exposure above 60 °C denatures enzymes and they lose their activity. To determine sufficient and optimum incubation durations and enzyme concentrations for degradation, cellulase at various concentrations and dosage regimes was added to 1 wt% CNF dispersions in sodium acetate buffer at pH 5, incubated at 50 °C, freeze dried, and analyzed for their degradation into glucose using <sup>1</sup>H-NMR spectroscopy in D<sub>2</sub>O (Table S1). Even after extensive degradation, samples did not completely dissolve in D<sub>2</sub>O as some solid segments remained. This solid content varied based on the time period that samples were allowed to degrade as samples were almost all solid after 1 h incubation, but almost a clear solution after 20 h. However, degradation did enable <sup>1</sup>H-NMR analysis of the CNF samples, yielding spectra where  $\alpha$ - and  $\beta$ -glucose were observed in the spectra (Fig. 3a).

Since the CNFs did not visibly completely degrade and that the enzymatic hydrolysis was not expected to convert all cellulose to glucose, the acetate peak at 1.88 ppm (Fig. 3) from the buffer was used as internal standard to find the degree of degradation by  $^1\text{H-NMR}$  spectroscopy. As shown in Table S1 the maximum degradation was achieved ( $\geq 85\%$ ) when two 10  $\mu\text{L}$  doses of enzyme was added to 1 mL of dispersion over 20 h at 50 °C. Similar maximum levels of degradation have been observed for other CNFs degraded with cellulases (Martin-Sampedro et al. 2012). To further



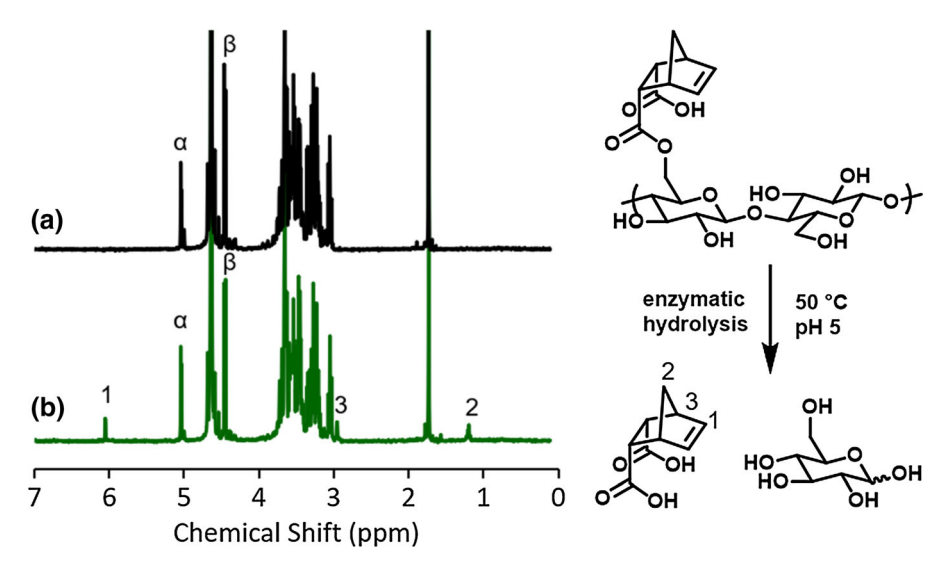


**Fig. 3** Enzymatic degradation of nCNFs under acidic condition and elevated temperature to produce both anomers of glucose units and 5-norbornene-2,3-dicarboxylic acid through hydrolysis of the ester under the acidic conditions. Representative <sup>1</sup>H-

NMR spectra of enzymatically degraded, **a** CNFs, **b** nCNFs. Peaks assignments are given for the anomeric protons of alpha and beta glucose as well as those for the norbornene group that are clearly visible

validate the method, a known amount of maleic anhydride was added to the CNF NMR samples as an independent standard and the results were consistent with using the acetate peak (Supporting Information, Fig. S2 and Table S1). This degradation method was used for all norbornene degree of functionalization measurements as the same degradation was achieved when nCNF samples were treaded with enzyme (80–100% degradation). Interestingly, CNF NMR samples could sit for a week in D2O at room temperature and the solid segments would disappear to yield a clear solution with a higher degree of degradation (ca. 95%), which suggests that the enzymes survived freeze-drying and retained activity. This degradation behavior is consistent with faster degradation (68 to 75% conversion after 5 h) of the amorphous regions of CNFs and then a slower degradation the crystalline regions (95% conversion after a week) (Mansfield and Meder 2003; Mandels et al. 1974).

Using the optimized degradation method, the degree of norbornene functionalization in nCNFs was calculated by  $^1\text{H-NMR}$  spectroscopy (Fig. 3b). The enzyme broke down the nCNFs into  $\alpha$ - and  $\beta$ -D-glucose units while the ester linkages between cellulose and norbornene group were hydrolyzed under the acidic conditions (pH 5) as evidenced by the sharp single peaks associated with the norbornene

dicarboxylic acid (1.3 ppm, 3.1 ppm, and 6.2 ppm). The degree of functionalization on an anhydroglucose repeat unit basis was calculated using the relative integration of norbornene and the glucose anomeric protons with a correction for the degree of CNF degradation (see Supporting Information for methods) to quantify how the concentration of carbic anhydride affected norbornene functionalization during synthesis (Fig. 2b). As demonstrated by the ATR-FTIR spectroscopy data, increasing the concentration of anhydride increases the norbornene functionality on nCNFs. At concentrations below 0.6 M, the functionalization degree doubled as the molarity of anhydride doubled; however, this trend was not observed when the concentration of carbic anhydride increased from 0.6 to 1.2 M. The degree of functionality plateaued at 0.6 M suggesting that the free hydroxyl groups on the surface of CNF were saturated much like what was inferred from the ATR-FTIR data. With this quantification method developed, nCNF samples with on average 10% functionality were used throughout the remainder of the study. This highest degree of functionality was used to promote more cross-linking reactions to improve the stability and modulus of resulting hydrogels.



nCNF hydrogel compression modulus control

CNF physical hydrogels are only held together by physical entanglements and hydrogen bonding interactions and thus, are known to lack long-term stability in aqueous systems (Hossen et al. 2018) because their interactions are dynamic. So, we hypothesized that thiol-norbornene cross-links could increase stability and control the modulus of the hydrogel in aqueous media. A short, small molecule cross-linker, 2,2'-(ethylenedioxy)diethanethiol) (DTDEG) was investigated at various thiol to norbornene ratios (T/NB) in a 4 wt% nCNF suspension using a UV-light radical initiator (I2959) (Fig. 1b). Due to light scattering from the fibrils, a 20-min irradiation time was used to ensure complete crosslinking of the hydrogel. Before exploring whether DTDEG cross-linking could be used to form stable and controllable nCNF hydrogels, we first ascertained whether it reacted with the surface norbornene groups on the CNFs. Hydrogels were synthesized at a T/NB of 2.5 using DTDEG, degraded in cellulase, and analyzed by <sup>1</sup>H-NMR spectroscopy, which indicated complete reaction of the norbornene group due to the complete disappearance of the protons associated with the alkene (Fig. S3). Moreover, new weak peaks were observed in the spectrum of the reacted nCNFs that corresponded to those for a model reaction between 5-norbornene-2,3-dicarboxylic acid and DTDEG (Fig. S3), which further confirms that the thiol-norbornene product was formed.

The ability to tune the compression modulus of hydrogels was investigated by varying the amount of the cross-linker added using the UV-initiated process. The non-cross-linked hydrogels (no DTDEG added), though holding their shape against gravity, tended to not resist against compression stress and were mostly untestable during compression testing as they would not provide sufficient resistance for the load cell to measure the force. This lack of dimensional stability of uncross-linked versus cross-linked nCNFs was underscored through observations of the hydrogels stored in PBS (Fig. S4). Some samples could be measured (Fig. 4a) without cross-linker (T/NB = 0) to give an approximation for the apparent stiffness of the native nCNFs. As demonstrated at Fig. 4a, higher T/NB values increased the compression modulus up to 6 kPa at its maximum for a T/NB of 1.2 and then decreased at higher T/NB. At T/NB greater than 1, the number of thiols exceeded the number of norbornenes, which saturates norbornene groups without forming effective cross-links. A similar phenomenon has been observed for soluble norbornene functionalized polymers suggesting that the same factors affect the crosslinking of nCNFs (Dadoo et al. 2017). Additionally, the maximum modulus was expected at T/NB equal to 1 since this should be a stoichiometrically balanced reaction and therefore yield the closest to ideal network. However, the maximum was observed at a T/NB of 1.2, which may be due to a systematic error with calculating the concentration of norbornenes by our method, the small molecule DTDEG not bridging the relatively long distance between norbornene groups on the surface of fibrils, or the formation of some disulfide linkages between DTDEG. In all cases, this reduction in cross-linking efficiency would be observed.

Pursuing the hypothesis that the distance between nCNFs prevented efficient DTDEG cross-linking, dithiol-terminated polyethylene glycol (DTPEG) samples with M<sub>n</sub> of 1.5 and 3 kg/mol were used to form hydrogels over the same range of T/NB as DTDEG. Unexpectedly, the same moduli as compared to the DTDEG hydrogels were obtained with these polymer cross-linkers under the same conditions (Fig. 4b). The compression modulus of a hydrogel is inversely related to the molecular weight between cross-links, which has been demonstrated for thiol-norbornene hydrogels (Jivan et al. 2016). Thus, using the higher molecular weight DTPEG cross-linkers could be expected to decrease the compression modulus for CNFs as compared to DTDEG if efficient cross-links were formed like those for soluble polymers. However, an opposite trend has been observed for TEMPO oxidized CNF hydrogels, where longer cross-linkers could span the gap between fibrils more efficiently and lead to higher modulus values (ca. 3 kPa) (Syverud et al. 2015). In our system, neither trend was observed and similar compression modulus values are seen as a function of T/NB regardless of the length of the crosslinker, which could be due to the nanoscale and micrometer scale hierarchical, fibrillar structure of nCNFs. On an equivalent weight basis in water as compared to soluble polymers or TEMPO oxidized CNFs, the distance between the fibrils for the mechanical refined material is greater because they are larger colloids with chains densely packed into a fibril, which leaves more distance between the fibrils



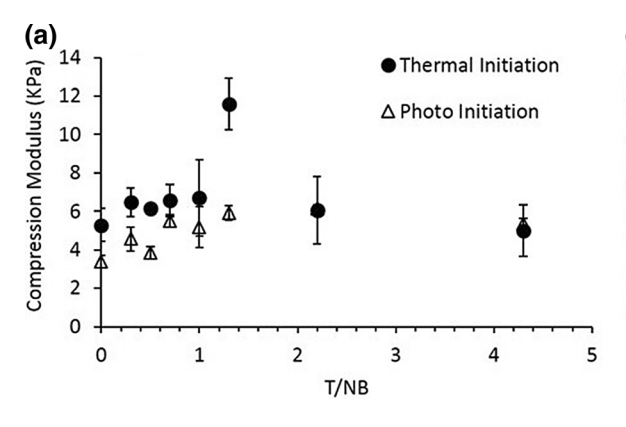
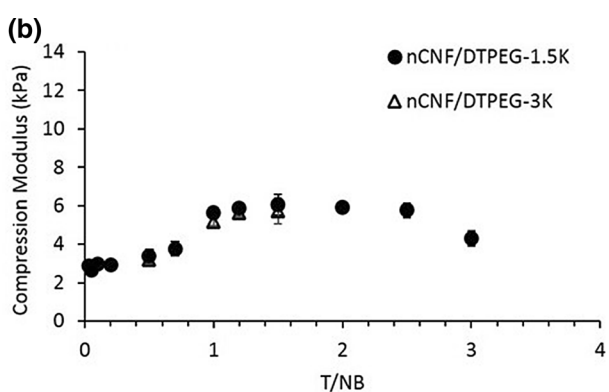


**Fig. 4 a** Compression modulus of nCNF-DTDEG hydrogels with varying T/NB values (4 wt% nCNFs) made by light initiated (triangles) (365 nm at 10 mW/cm² for 20 min) and thermal initiated (circle) gelation system (10 mM APS/TEMED at 37 °C for 3 h). **b** Compression modulus of nCNF-DTPEG-

as compared to smaller colloids. Thus, a dithiol may be more likely to react to norbornenes on the same fibril as opposed to creating a link between two different fibrils, so the cross-linking between fibrils is not as effective. Some fibril-fibril linkages must be created, though, because an increase in modulus and mechanical stability is observed.

Another possible explanation for the small modulus changes after cross-linking was that the UV light could be scattered by the CNFs, which would significantly reduce the effective light power and prevent cross-link formation. To overcome the potential scattering, thermal radical initiation was explored using the redox initiator pair APS/TEMED. The compression modulus values of these samples were slightly higher than UV-initiated samples (Fig. 4a) for all the T/NB values except for T/NB = 1.2, which doubled (12 kPa). This slight increase in modulus with redox initiators suggests that the small changes to modulus during cross-linking was not likely related to UV light scattering by the dispersion. Of note, during the incubation samples would visibly contract and shrink due to water evaporation when using the same molds for the UV irradiation. The samples could regain the original mold dimensions if placed in PBS after gelation (see Table S2 in Supporting Information). This shrinking could explain why a T/NB of 1.2 yielded a significantly higher modulus as the contraction during the reaction brought fibrils closer to each other so that they were more likely to form cross-links due to the higher local concentration. This behavior



1.5 k (circle, 1.5 kg/mol DTPEG) and nCNF-DTPEG-3 k (triangle, 3.0 kg/mol DTPEG) UV-initiated hydrogels at several T/NB values (4 wt% nCNFs, 365 nm at 10 mW/cm² for 20 min). Error bars are standard deviations (n  $\geq$  5). Hydrogels were 4.5 mm in diameter and a total of 50  $\mu L$  in volume

was further underscored by 3 wt% nCNFs APS/ TEMED initiated hydrogels yielding higher modulus values than those with 4 wt% nCNFs (Fig. S5). These results are consistent with contraction improving the fibril-fibril linkages since the 3 wt% hydrogels shrank more than the 4 wt% while heating to bring the fibrils closer to each other. The 3 wt% hydrogels likely shrank to a greater extent because the lower solids content reduced hydrogen bonding between water and nCNF surfaces and therefore, more free water that was easier to evaporate. This water evaporation led to the contraction of the hydrogels due to capillary forces. For both the 3 and 4 wt% APS/TEMED initiated samples, the shrinking during crosslinking appears to enable more successful chemical crosslinks, but does not cause hysteresis of the hydrogels as they reswell back the original mold's dimensions, yielding the same original CNF concentrations in the hydrogel. These results demonstrate some inherent challenges with adjusting the modulus of covalently cross-linked, primarily CNF hydrogels due to the large fibril-fibril distances in suspension and suggest that cross-linking in a collapsed state can lead to greater modulus values and control. Additionally, although varying the T/NB did not provide a large range of compression modulus when using the UV-initiator, the process enhanced modulus and added dimensional stability in aqueous media.



## Rheological behavior of hydrogels

Our previous work showed that norbornene functionalization on CNFs lead to reduced fibril-fibril interactions, which reduces the viscosity of dilute suspensions (Fein et al. 2020). To further explore the nature of the nCNFs and the hydrogels that were formed through thiol-norbornene reactions, their rheological behavior was studied. At low frequency (1 Hz) and strain (1%) the CNFs (Fig. S6) and nCNFs (Fig. 5a) behaved as solids since the storage modulus (G') is higher than the loss modulus (G''). The modification of CNFs to nCNFs significantly reduced the storage modulus by half (14 kPa to 7 kPa at 4 wt%), which is consistent with our previous findings that the norbornene functionalization disrupts the fibril-fibril interactions that lead to the physical CNF network. When the nCNF content was reduced from 4 to 3 wt%, an interesting consequence was that the storage modulus at low strains dropped by orders of magnitude (Fig. 5a). The same change in solids content did not have as drastic an effect on the storage modulus of the CNF suspension (Fig. S6), which further supports the norbornene functionalization of CNFs significantly altered how the fibrils interact with each other. However, at low strain, the storage modulus did not change with frequency (1–10 Hz), which indicated that these are physically entangled to form a hydrogel. As expected, both CNFs and nCNFs demonstrated shear thinning behavior demonstrated by G" surpassing G' at high strain (Fig. 5a and S6) (Lotti et al. 2011).

Rheological measurements of the storage modulus of thermally gelled samples also showed that varying the T/NB did not cause large changes to the modulus, yielding a doubling over native nCNFs to 13-15 kPa at all T/NB values tested (Fig. S7). Strain sweeps of the nCNF hydrogels confirmed incomplete crosslinking occurred because the samples yielded at high strain values, indicating the samples were still shear thinning (Fig. S8). However, these rheological measurements did confirm the visible observation that nCNF hydrogels were more stable than the native CNF and nCNF suspensions since the hydrogel yield strains (strain where G'' becomes greater than G') were higher (ca. 25% for the suspensions in Fig. S6 and 60% for the hydrogel at 3 wt% solids). These rheological measurements support the findings that cross-linking nCNFs stabilize the physical network by adding in effective covalent cross-links.

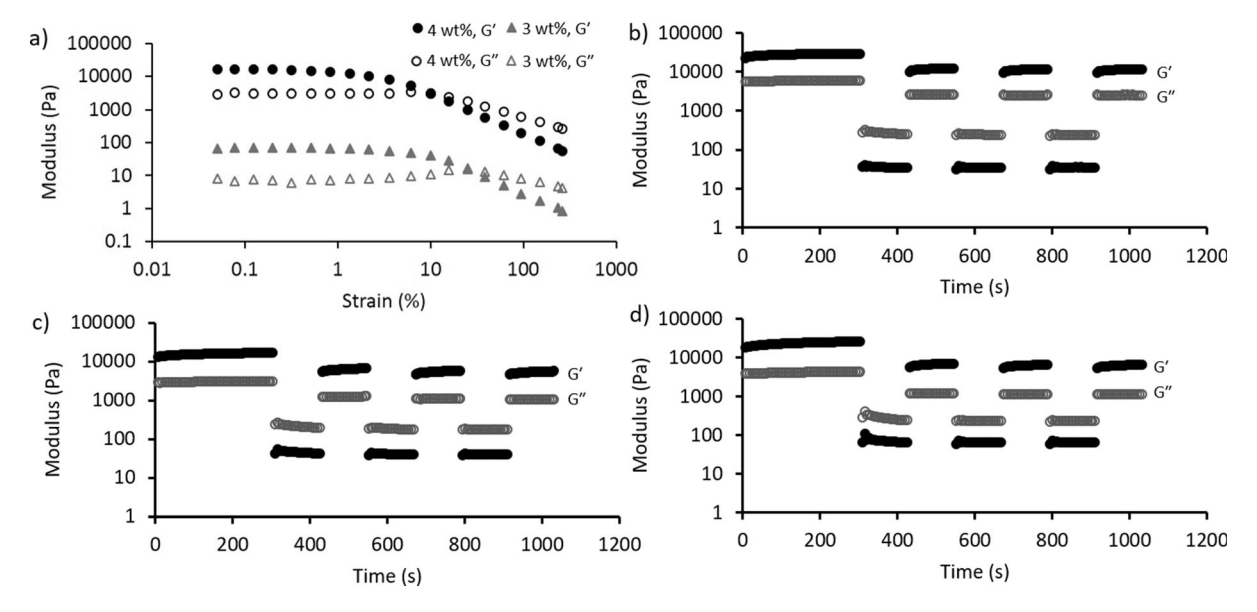


**Fig. 5** Rheological behavior of CNFs, nCNFs, and thermally gelled nCNF-DTDEG hydrogels (T/NB = 1, 10 mM APS/TEMED, 3 h gelation at 37 °C). **a** Strain sweep at 1 Hz for 3 wt% (gray triangles) and 4 wt% (black circles) nCNF suspensions at 37 °C where closed symbols indicate G' and open symbols indicate G''. Oscillatory strain step shear thinning

measurements at 10 Hz with alternating low (0.5%) and high (250%) strain in 2 min increments (after an initial 5 min equilibration) for 4 wt% suspensions of **b** CNFs, **c** nCNFs, **d** nCNF-DTDEG hydrogel at 37 °C. Closed symbols indicate G' and open symbols indicate G"



CNF aqueous dispersions are shear-thinning materials (Lotti et al. 2011; Karppinen et al. 2012) due to physical fibril-fibril interactions, which have enabled their use as injectable scaffolds for regeneration and cell culture (Rashad et al. 2017; Kuzmenkoa et al. 2018). Since all materials demonstrated a shear thinning nature, we explored whether this shear thinning was recoverable and repeatable for CNFs, nCNFs, and a thermally cross-linked nCNF-DTDEG hydrogel at T/NB equal to one, using oscillatory strain step experiments (Figs. 5b, c). All three samples exhibit a shear-thinning character when they initially were sheared to 250% strain as their storage modulus reduced by three orders of magnitude. When the strain was reduced back to 0.5%, all samples did not fully recover back to their initial modulus values from when they were originally loaded into the rheometer. CNFs and nCNFs recovered 40% of their modulus and the nCNF-DTDEG recovered only 27% of the value. This modulus loss suggests that the network and/or fibrilfibril interactions are different upon the initial application of high shear, which may be due to the fibrils finding an equilibrium state upon application of high shear or some thiol-ether linkages breaking. However, subsequent high shear steps did not reduce the low shear storage modulus from this new value and less than 20 s at low strain was required to reach 90% of the previous low strain storage modulus (Figs. 5b-d). This same behavior was observed for the lower solids content materials as well (Fig. S9). The storage modulus for the 3 wt% hydrogel measured on the rheometer was significantly lower than that measured for compression modulus, which was likely due to the fact that the hydrogel was formed between the geometry and the plate, reducing shrinkage and chemical crosslinks from being formed. The shear thinning character and the rapid recovery of modulus is consistent with fibrils entangling at low strain and under shear aligning to flow (Lotti et al. 2011). The initial reduction of storage modulus could be as a result of hydrogen bond formation between aligned fibrils that is broken with the initial shear (Lotti et al. 2011). The recovery of nCNFs and nCNF-DTDEG modulus also showed that functionalization and even thiol-norbornene cross-linking did not completely change the interactions between fibrils. The shear thinning behavior of the nCNF-DTDEG hydrogels also confirms that the materials are not completely cross-linked, but rather the thiol-norbornene reaction

links some number of fibrils together that decreases overall mobility of the fibrils and subsequently increases the stability of the physical hydrogel in water.

#### **Conclusions**

Using a straightforward procedure, mechanically refined, hydroxyl functionalized CNFs could be modified with pendent norbornene groups. The degree of functionalization could be controlled by varying the concentration of 5-norbornene-2,3-dicarboxylic anhydride in reaction media to a point at which the degree of functionalization plateaued. Though relative functionalization could be tracked with infrared spectroscopy, enzymatic degradation of the nCNFs with subsequent <sup>1</sup>H-NMR analysis could be used to quantify the actual degree of functionalization. The nCNFs reacted with dithiol cross-linkers under UV-light stabilized CNF hydrogels in aqueous environments and controlled hydrogel compression modulus, which could enable these materials for biomedical and sustainable material applications. The length of dithiol cross-linker did not affect compression modulus, which was likely due to challenges associated with the cross-linker spanning the distance between fibrils to form effective cross-links. Thermal gelation with dimensional contraction brought fibrils closer together so they could form effective cross-links and subsequently higher modulus values. Though stabilized, nCNF hydrogels still exhibited shear thinning behavior consistent with an incomplete chemical network.

Acknowledgments The work was supported by the National Science Foundation funded REU Site Explore it! Building the Next Generation of Sustainable Forest Bioproduct Researchers (EEC-1461116 and EEC- 1757529) and University of Maine Research Reinvestment Fund support through the Vice President for Research at the University of Maine.

#### References

Azoidis I, Metcalfe J, Reynolds J, Keeton S, Hakki SS, Sheard J, Widera D (2017) Three-dimensional cell culture of human mesenchymal stem cells in nanofibrillar cellulose hydrogels. MRS Commun 7:458–465

Balasubramanian N, Nelson S (2014) Bacillus pumilus S124A carboxymethyl cellulase; a thermo stable enzyme with a



- wide substrate spectrum utility. Int J Biol Macromol 67:132-139
- Basu A, Celma G, Stromme M, Ferraz N (2018) In vitro and in vivo evaluation of the wound healing properties of nanofibrillated cellulose hydrogels. ACS Appl Bio Mater 1:1853–1863
- Berto GL, Arantes V (2019) Kinetic changes in cellulose properties during defibrillation into microfibrillated cellulose and cellulose nanofibrils by ultra-refining. Int J Bio Macromol 127:637–648
- Bhattacharya M, Malinen MM, Lauren P, Lou Y-R, Kuisma SW, Kanninen L, Niklander T, Noon J, Lille M, Corlu A, GuGuen-Guillouzo Ch, Ikkala O, Urtti A, Laukkanen A, Yliperttula M (2012) Nanofibrillar cellulose hydrogel promotes three-dimensional liver cell culture. J Control Release 164:291–298
- Bozic M, Vivod V, Kavcic S, Leitgeb M, Kokol V (2015) New findings about the lipase acetylation of nanofibrillated cellulose using acetic anhydride as acyl donor. Carbohydr Polym 125:340–351
- Brown TE, Anseth KS (2017) Spatiotemporal hydrogel biomaterials for regenerative medicine. Chem Soc Rev 46:6532–6552
- Caliari SR, Vega SL, Kwon M, Soulas EM, Burdick JA (2016)
  Dimensionality and spreading influence MSC YAP/TAZ
  signaling in hydrogel environments. Biomaterials
  103:314–323
- Campodoni E, Heggset EB, Rashad A, Ramirez-Rodriguez GB, Mustafa K, Syverud K, Tampieri A, Sandri M (2019) Polymeric 3D scaffolds for tissue regeneration: Evaluation of biopolymer nanocomposite reinforced with cellulose nanofibrils. Mater Sci Eng C 94:867–878
- Chin K-M, Ting SS, Ong HL, Omar M (2018) Surface functionalized nanocellulose as a veritable inclusionary material in contemporary bioinspired applications: a review. J Appl Polym Sci 2018:46065
- Courtenay JC, Ramalhete SM, Skuze WJ, Soni R, Khimyak YZ, Edler KJ, Scott JL (2018) Unravelling cationic cellulose nanofibril hydrogel structure: NMR spectroscopy and small angle neutron scattering analyses. Soft Matter 14:255–263
- Curvello R, Raghuwanshi VS, Garnier G (2019) Engineering nanocellulose hydrogels for biomedical applications. Adv Colloid Interface Sci 267:47–61
- Dadoo N, Landry SB, Bomar JD, Gramlich WM (2017) Synthesis and spatiotemporal modification of biocompatible and stimuli responsive carboxymethyl cellulose hydrogels using thiol-norbornene chemistry. Macromol Biosci 17:1700107
- De France KJ, Hoare T, Cranston ED (2017) Review of hydrogels and aerogels containing nanocellulose. Chem Mater 29:4609–4631
- Deng S, Binauld S, Mangiante G, Frances JM, Charlot J, Bernard J, Zhou X, Fleury E (2016) Microcrystalline cellulose as reinforcing agent in silicone elastomers. Carbohydr Polym 151:899–906
- Deng Z, Jung J, Simonsen J, Zhao Y (2017) Cellulose nanomaterials emulsion coatings for controlling physiological activity, modifying surface morphology, and enhancing storability of postharvest bananas (Musa acuminate). Food Chem 232:359–368

- Diniz F, Castro G (2004) Hornification—its origin and interpretation in wood pulps. Wood Sci Technol 37:489–494
- Doench I, Torres-Ramos MEW, Montembault A, de Olveira PN, Halimi C, Viguier E, Heux L, Siadous R, Thire RMSM, Osorio-Madrazo A (2018) Injectable and gellable chitosan formulations filled with cellulose nanofibers for intervertebral disc tissue engineering. Polymers 10:1202
- Dong H, Snyder JF, Williams KS, Andzelm JW (2013) Cationinduced hydrogels of cellulose nanofibrils with tunable moduli. Biomacromol 14(9):3338–3345
- Erlandsson J, Pettersson T, Ingverud T, Granberg H, Larsson PA, Malkoch M, Wagberg L (2018) On the mechanism behind freezing-induced chemical cross-linking in ice-templated cellulose nanofibril aerogels. J Mater Chem A 6:19371–19380
- Espinosa E, Rol F, Bras J, Rodriguez A (2019) Production of lignocellulose nanofibers from wheat straw by different fibrillation methods. Comparison of its viability in cardboard recycling process. J Clean Prod 239:118083
- Fein K, Bousfield DW, Gramlich WM (2020) The influence of versatile thiol-norbornene modifications to cellulose nanofibers on rheology and film properties. Carbohydr Polym 230:115672
- Filpponen I, Argyropoulos DS (2010) Regular linking of cellulose nanocrystals via click chemistry: synthesis and formation of cellulose nanoplatelet gels. Biomacromol 11:1060–1066
- Fu L-H, Qi C, Ma M-G, Wan P (2019) Multifunctional cellulose-based hydrogels for biomedical applications. J Mater Chem B 7:1541–1562
- Gordeyeva KS, Fall AB, Hall S, Wicklein B, Bergstrom L (2016) Stabilizing nanocellulose-nonionic surfactant composite foams by delayed Ca-induced gelation. J Colloid Interface Sci 472:44–51
- Gramlich WM, Kim IL, Burdick JA (2013) Synthesis and orthogonal photopatterning of hyaluronic acid hydrogels with thiol-norbornene chemistry. Biomaterials 34:9803–9811
- Heggset EB, Strand BL, Sundby KW, Simon S, Chinga CG, Syverud K (2019) Viscoelastic properties of nanocellulose based inks for 3D printing and mechanical properties of CNF/alginate biocomposite gels. Cellulose 26:581–595
- Hoeng F, Denneulin A, Krosnicki G, Bras J (2016) Positive impact of cellulose nanofibrils on silver nanowire coatings for transparent conductive films. J Mater Chem C 4:10945–10954
- Hossen MR, Dadoo N, Holomakoff DG, Co A, Gramlich WM, Mason MD (2018) Wet stable and mechanically robust cellulose nanofibrils (CNF) based hydrogel. Polymer 151:231–241
- Jivan F, Yegappan R, Pearce H, Carrow JK, McShane M, Gaharwar AK, Alge DL (2016) Sequential thiol-ene and tetrazine click reactions for the polymerization and functionalization of hydrogel microparticles. Biomacromol 17:3516–3523
- Kargarzadeh H, Huang J, Lin N, Ahmad I, Mariano M, Dufresne A, Thomas S, Galeski A (2018) Recent developments in nanocellulose-based biodegradablepolymers, thermoplastic polymers, and porous nanocomposites. Prog Polym Sci 87:197–227



- Karppinen A, Saarinen T, Salmela J, Laukkanen A, Nuopponen MS (2012) Flocculation of microfibrillated cellulose in shear flow. Cellulose 19:1807–1819
- Kato KL, Cameron RE (1999) A review of the relationship between thermally-accelerated ageing of paper and hornification. Cellulose 6:23–40
- Khalil HPSA, Davoudpour Y, Islam MN, Mustapha A, Sudesh K, Dungani R, Jawaid M (2014) Production and modification of nanofibrillated cellulose using various mechanical processes: A review. Carbohydr Polym 99:649–665
- Kong W, Wang C, Jia C, Kuang Y, Pastel G, Chen C, Chen G, He S, Huang H, Zhang J, Wang S, Hu L (2018) Muscleinspired highly anisotropic, strong, ion-conductive hydrogels. Adv Mater 30:1801934
- Kuzmenkoa V, Karabuluta E, Pernevikc E, Enokssona P, Gatenholma P (2018) Tailor-made conductive inks from cellulose nanofibrils for 3D printing of neural guidelines. Carbohydr Polym 189:22–30
- Lin C-C, Ki CS, Shih H (2015) Thiol-norbornene photoclick hydrogels for tissue engineering applications. J Appl Polym Sci 132:41563
- Liu J, Chinga-Carrasco G, Cheng F, Xu W, Willfor S, Syverud K, Xu C (2016) Hemicellulose-reinforced nanocellulose hydrogels for wound healing application. Cellulose 23:3129–3143
- Lojewska J, Miskowiec P, Lojewski T, Proniewicz LM (2005) Cellulose oxidative and hydrolytic degradation: In situ FTIR approach. Polym Degrad Stability 88:512–520
- Lotti M, Gregersen ØW, Moe S, Lenes M (2011) Rheological studied of macrofibrillar cellulose water dispersions. J Polym Environ 19:137–145
- Lou Y-R, Kanninen L, Kuisma T, Niklander J, Noon LA, Burks D, Urtti A, Yliperttula M (2014) The use of nanofibrillar cellulose hydrogel as a flexible three-dimensional model to culture human pluripotent stem cells. Stem Cells Devel 23(4):380–392
- Mandels M, Hontz L, Nystrom J (1974) Enzymatic hydrolysis of waste cellulose. Biotechnol Bioeng 16:1471–1493
- Mansfield S, Meder R (2003) Cellulose hydrolysis—the role of monocomponent cellulases in crystalline cellulose degradation. Cellulose 10:159–169
- Mariano M, Hantao LW, da Silva BJ, Strauss M (2018) Microstructural characterization of nanocellulose foams prepared in the presence of cationic surfactants. Carbohydr Polym 195:153–162
- Martin-Martinez F, Jin K, Lopez Barreiro D, Buehler MJ (2018)
  The rise of hierarchical nanostructured materials from renewable sources: learning from nature. ACS Nano 12:7425–7433
- Martin-Sampedro R, Filpponen I, Hoeger IC, Zhu JY, Laine J, Rojas OJ (2012) Rapid and complete enzyme hydrolysis of lignocellulosic nanofibrils. ACS Macro Letters 1:1321–1325
- Mathew AP, Oksman K, Pierron D, Harmand M-FO (2012) Fibrous cellulose nanocomposite scaffolds prepared by partial dissolution for use as ligament or tendon substitutes. Carbohydr Polym 87:2291–2298
- McCall JD, Anseth KS (2012) Thiol-ene photopolymerizations provide a facile method to encapsulate proteins and maintain their bioactivity. Biomacromol 13:2410–2417

- McOscar TVC, Gramlich WM (2018) Hydrogels from norbornene-functionalized carboxymethyl cellulose using a UV-initiated thiol-ene click reaction. Cellulose 25:6531–6545
- Moon RJ, Martini A, Nairn J, Simonsen J, Youngblood J (2011) Cellulose nanomaterials review: structure, properties and nanocomposites. Chem Soc Rev 40:3941–3994
- Moon RJ, Schueneman GT, Simonsen J (2016) Overview of cellulose nanomaterials, their capabilities and applications. JOM 68:2383–2394
- Navarro JRG, Edlund U (2017) Surface-initiated controlled radical polymerization approach to enhance nanocomposite integration of cellulose nanofibrils. Biomacromol 18:1947–1955
- Nechyporchuk O, Pignon F, Belgacem MN (2015) Morphological properties of nanofibrillated cellulose produced using wet grinding as an ultimate fibrillation process. J Mater Sci 50:531–541
- Nishiguchi A, Taguchi T (2019) Osteoclast-responsive, injectable bone of bisphosphonated-nanocellulose that regulates osteoclast/osteoblast activity for bone regeneration. Biomacromol 20:1385–1393
- Niu J, Wang J, Dai X, Shao Z, Huang X (2018) Dual physically cross-linked healable polyacrylamide/cellulose nanofibers nanocomposite hydrogels with excellent mechanical properties. Carbohydr Polym 193:73–81
- Oksman K, Mathew AP, Sain M (2009) Novel bionanocomposites: processing, properties and potential applications. Plast Rubbers Compos 38(9–10):396–405
- Ooi HW, Hafeez S, van Blitterswijk CA, Moroni L, Baker MB (2017) Hydrogels that listen to cells: a review of cell-responsive strategies in biomaterial design for tissue regeneration. Mater Horiz 4:1020–1040
- Otoni CG, Carvalho AS, Cardoso MVC, Bernardinelli OD, Lorevice MV, Colnago LA, Loh W, Mattoso LHC (2018) High-pressure microfluidization as a green tool for optimizing the mechanical performance of all-cellulose composites. ACS Sustain Chem Eng 6:12727–12735
- Rashad A, Mustafa K, Heggset EB, Syverud K (2017) Cytocompatibility of wood-derived cellulose nanofibril hydrogels with different surface chemistry. Biomacromol 18:1238–1248
- Rodell CB, Kaminski AL, Burdick JA (2013) Rational design of network properties in guest-host assembled and shearthinning hyaluronic acid hydrogels. Biomacromol 14(11):4125–4134
- Rol F, Belgacem MN, Gandini A, Bras J (2019) Recent advances in surface-modified cellulose nanofibrils. Prog Polymer Sci 88:241–264
- Saini S, Falco CY, Belgacem MN, Bras J (2016) Surface cationized cellulose nanofibrils for the production of contact active antimicrobial surfaces. Carbohydr Polym 135:239–247
- Salari M, Bitounis D, Bhattacharya K, Pyrgiotakis G, Zhang Z, Purington E, Gramlich WM, Grondin Y, Rogers R, Bousfield D, Demokritou P (2019) Development and characterization of fluorescently tagged nanocellulose for nanotoxicological studies. Environ Sci Nano 6:1516–1526
- Satyamurthy P, Jain P, Karande VS, Nadanathangam V (2016) Nanocellulose induces cellulase production in *Tricho-derma reesei*. Process Biochem 51:1452–1457



- Sharma PR, Zheng B, Sharma SK, Zhan CZ, Wang R, Bhatia SR, Hsiao BS (2018) High Aspect ratio carboxycellulose nanofibers prepared by nitro-oxidation method and their nanopaper properties. ACS Appl Nano Mater 1:3969–3980
- Shinner F, Von Mersi W (1990) Xylanase-CM-cellulase—and invertase activity in soil: an improved method. Soil Boil Biochem 22(4):511–515
- Spence KL, Venditti RA, Rojas OJ, Habibi Y, Pawlak JJ (2011) A comparative study of energy consumption and physical properties of microfibrillated cellulose produced by different processing methods. Cellulose 18:1097–1111
- Syverud K, Kirsebom H, Hajizadeh S, Chinga-Carrasco G (2011) Cross-linking cellulose nanofibrils for potential elastic cryo-structured gels. Nanoscale Res Lett 6:626
- Syverud K, Pettersen SR, Draget K, Chinga-Carrasco G (2015) Controlling the elastic modulus of cellulose nanofibril hydrogels-scaffolds with potential in tissue engineering. Cellulose 22:473–481
- Tomic S, Kokol V, Mihajlovic D, Mircic A, Colic M (2016) Native cellulose nanofibrills induce immune tolerance in vitro by acting on dendritic cells. Sci Rep 6:31618
- Vinzant TB, Adney WS, Decker SR, Baker JO, Kinter MT, Sherman NE, Fox JW, Himmel ME (2001) Fingerprinting trichoderma reesei hydrolases in a commercial cellulase preparation. Appl Biochem Biotech 91–93:99–107
- Vuoti S, Talja R, Johansson L-S, Heikkinen H, Tammelin T (2013) Solvent impact on esterification and film formation ability of nanofibrillated cellulose. Cellulose 20:2359–2370
- Wang L, Sanders JE, Gardner DG, Han Y (2016) In-situ modification of cellulose nanofibrils by organosilanes during spray drying. Industrial Crops Prod 93:129–135
- Wang J, Hua B, Wang X, Cui Z (2017) Characteristics of cellulase in cellulose-degrading Bacterium strain Clostridium straminisolvens (CSK1). Afr J Microbiol Res 11(10):414–421

- Xu W, Molino BZ, Cheng F, Molino PJ, Yue Z, Su D, Wang X, Willfor S, Xu C, Wallace GG (2019) On low-concentration inks formulated by nanocellulose assisted with gelatin methacrylate (GelMA) for 3D printing toward wound healing application. ACS Appl Mater Interfaces 11:8838–8848
- Xu W, Zhang X, Yang P, Langvik O, Wang X, Zhang Y, Cheng F, Osterberg M, Willfor S, Xu C (2019) Surface engineered biomimetic inks based on UV cross-linkable wood biopolymers for 3D printing. ACS Appl Mater Interfaces 11:2389–12400
- Yang J, Xu F (2017) Synergistic reinforcing mechanisms in cellulose nanofibrils composite hydrogels: interfacial dynamics, energy dissipation, and damage resistance. Biomacromol 18:2623–2632
- Yang X, Abe K, Biswas SK, Yano H (2018) Extremely stiff and strong nanocomposite hydrogels with stretchable cellulose nanofiber/poly(vinyl alcohol) networks. Cellulose 25:6571–6580
- Yuan B, Zhang J, Mi Q, Yu J, Song R, Zhang J (2017) Transparent cellulose-silica composite aerogels with excellent flame retardancy via an in situ sol-gel process. ACS Sustainable Chemistry & Engineering 5:11117–11123
- Zander NE, Dong H, Steele J, Grant JT (2014) Metal cation cross-linked nanocellulose hydrogels as tissue engineering substrates. ACS Appl Mater Interfaces 6(21):18502–18510
- Zhang H, Lyu S, Zhou X, Gu H, Ma C, Wang C, Ding T, Shao Q, Liu H, Guo Z (2019) Super light 3D hierarchical nanocellulose aerogel foam with superior oil adsorption. J Colloid Interface Sci 536:245–251

**Publisher's Note** Springer Nature remains neutral with regard to jurisdictional claims in published maps and institutional affiliations.

